Numerical Simulation of Wind Load on Prefabricated Buildings Using Computational Fluid Dynamics

Yin Li* and Ang Wang

Huanghe Science and Technology College, Henan, 450000, China

* Corresponding Author Email: hkdliyin@163.com

Abstract. At present, the wind tunnel experiment is more and more widely used, but it is rarely used in the construction industry. Therefore, this thesis is to study the wind load of prefabricated buildings by numerical simulation. First, the application field of wind load numerical simulation is analyzed. Next, the numerical model is used to simulate the average wind pressure distribution on the building surface of single tower, tower G and tower F. The turbulence model is established based on fluid mechanics, which makes the obtained data more accurate and can converge quickly. Finally, the wind load interference effects of two fabricated towers and a single tower are analyzed. The experimental results show that the moment coefficient interference factor of tower F remains between 0.696~1.125 and that of tower G remains between 0.291~1.043. When the wind direction angle is 90°, the maximum values of the building base torque and the base bending moment around the X axis appear simultaneously, and the moment around the Y axis is not 0, which will change the stress of the building on the base. If the wind direction angle becomes 0°, the two fabricated towers will interact to reduce the impact on the base moment of the upstream building. Meanwhile, the wind pressure interference factor on the wall surface of prefabricated buildings remains between [-1, 1.5]. When the buildings in the upstream are blocked, the wind pressure interference factor may become 0. However, the shape coefficient of negative pressure on the inner wall of the building will increase rapidly due to the narrow channel effect. This thesis will analyze the wind load on the surface of prefabricated buildings through numerical simulation, which will help the wind engineering team build safer prefabricated buildings.

Keywords: fluid mechanics; prefabricated buildings; wind load; numerical simulation; moment.

1. Introduction

Since the 21st century, various building technologies have developed rapidly. Different types of houses and buildings have emerged, from single buildings in the past to high-rise, super high-rise, and towering building structures at present [1]. Especially in the construction of first-tier cities, high-rise and super-high-rise buildings have become the first choice and the mainstream trend in the future. It reveals that the architectural style of the society is gradually developing towards softer and higher [2]. Besides, the resources actually used for agricultural farmland in the current society are pretty scarce, and most of these lands are located around the city. After a long period of rapid development, the number of agricultural lands has become one of the main factors restricting the current socio-economic development. In response to the sustainable development strategy advocated by the country, people must cherish the use of land in urban construction. Thereby, the city's three-dimensional (3D) space should be used [3]. The current society has entered the rapid development process of urban high-rise buildings, and various high-rise buildings have sprung up in major cities. With the continuous extension of urban buildings in 3D space, the stiffness of the building structure becomes smaller and smaller, and the wind load gradually becomes the control load. When designing super-high-rise buildings with complex internal structures, there are no relevant provisions on wind load at this stage. However, such buildings are highly sensitive to wind loads, which requires designers to pay special attention to the wind resistance of the buildings [4].

Ritos et al. (2018) studied the performance of parallel implicit Large Eddy Simulations (iLES) combined with higher-order weighted basically non-oscillatory schemes, with an accuracy of 11 orders. The Taylor Green vortex and supersonic turbulent boundary layer flow were simulated on High Performance Computing (HPC) equipment. The current iLES is highly scalable, achieving

about 93% and 68% performance on 1536 and 6144 cores, respectively, for the simulation of about 1.07 billion cell grids. The research also shows that the higher-order iLES have achieved similar accuracy with the strict Direct Numerical Simulation (DNS) under low computational cost [5]. Farmakis et al. (2020) proposed that the key feature of the current relaxed Multi-dimensional Optimal Order Detection (MOOD) equation is that the Numerical Admissible Detector (NAD) is not the only defined order of all spatial accuracy. Moreover, it is relaxed when reaching second-order accuracy. The numerical scheme was applied to a two-dimensional unsteady Euler equation, and multiple experimental problems such as two-dimensional vortex evolution, cylinder explosion, double Mach reflection and implosion were calculated. It reveals that in many cases, the implemented MOOD example tries to maintain the symmetry of the formed structure in the simulation, which is an improvement compared with the non-MOOD limited research and design. Because of the multi-dimensional reconstruction nature of the scheme, it is not easy to obtain [6]. Niu (2021) studied the wind load and flow field structure around the Parabolic Trough Collectors (PTC) array by using the Delayed Detached Eddy Simulation (DDES) method. The scaled 3D model was adopted and stimulated through ANSYS-fluent software. The first PTC in the array experiences the maximum average pressure on the windward side of the model, corresponding to the maximum average resistance coefficient. The comparison of flow patterns around PTC shows that when the pitch angle $\theta=0°$ and $\theta=180°$, the vorticity concentration in front of the collector is high [7].

To sum up, research teams worldwide are using numerical simulation methods to gradually expand the scope of application of wind tunnel tests, which is no longer limited to the aviation field. However, there are few applications in the field of architecture. Considering that there are more and more high-rise buildings in first-tier cities, the research on prefabricated buildings has become essential. Hence, numerical simulation analysis of the wind load of prefabricated buildings in cities will be conducted through fluid mechanics. First, the wind load numerical simulation of the building is analyzed. Then, the related wind load data are analyzed by establishing a numerical model and turbulence model. The research innovation is to combine turbulence model and numerical model, making the obtained data more accurate and the conclusion more convincing. It is hoped that the research results can improve the safety of urban high-rise buildings and provide a reference for the research team in the construction industry.

2. Research scheme design

2.1 Numerical simulation of wind load

Wind load is one of the crucial loads that designers cannot ignore in designing ground buildings. In the construction of high-rise buildings, wind load is a factor that designers must pay attention to. With the increasing proportion of high-rise buildings in the city, the wind resistance design of high-rise buildings has become one of the first factors that designers must consider [8, 9]. How to accurately calculate the wind load of high-rise buildings has become the first step of wind resistance design. At present, the wind load data are obtained mainly by implementing the model of urban high-rise buildings and conducting wind tunnel experiments on them. In recent years, relevant wind tunnel research teams have combined computer and fluid dynamics to find a numerical wind tunnel method to realize the accurate calculation of wind load. Compared with the traditional wind tunnel experiment, the numerical wind tunnel has a lower cost and shorter cycle, and can also realize the complete recording, observation and reproduction of various physical quantities at the monitoring points. Due to these advantages, in the last three decades, numerical wind tunnel has been favored by multiple industries, especially in the construction industry. Now, many laboratories use wind tunnel experiments as an auxiliary method to calculate the wind load of high-rise buildings [10]. Numerical calculation and fluid mechanics are the theoretical basis of the numerical wind tunnel. Fluid dynamics mainly uses differential equations to simulate fluid motion, but the process of calculating fluid differential equations is extremely complex. Differential equations must be transformed into algebraic equations to get results. A numerical wind tunnel is to discretize the watershed space through grids,

and then adjust the differential equations established in fluid dynamics to algebraic equations. Finally, the numerical method is used to get the solution and obtain the wind pressure and wind speed data of the flow field [11]. At the early stage, society as a whole mainly applied computational fluid dynamics in the aviation field, so fluid mechanics was first successfully applied in the aviation field. Then, when it is applied to structural wind engineering, it encounters many difficulties. Compared with the shape of space vehicles, the structures of urban high-rise buildings are mostly blunt bodies, which are more complex than streamlined aircraft [12, 13].

2.2 Numerical model

A. Project introduction

The researched project is an S comprehensive transportation hub project, including two super-high-rise office buildings with the same shape and symmetrical layout, which belong to the urban area with dense high-rise buildings. The safety level of the building structure in this area is Grade II. The building looks like a rectangle. After measurement, the distance between the two buildings is 46m, the height of the building from the ground is 220m, and the section size of the building is 46m × 40m. The buildings are two adjacent super-high-rise towers, and there is an obvious interference effect between the two towers (tower F and tower G). Therefore, it is necessary to determine the wind load value of the building surface through numerical simulation [14-16]. Since the structure and building layout are symmetrical, Fluent 14.5 software will be used to simulate the wind pressure distribution on the building surface in five different wind directions of 0°, 22.5°, 45°, 67.5° and 90°. Meanwhile, under the same working conditions, the average wind pressure distribution on the building surface when the single tower is arranged is numerically simulated [17].

B. Computing domain and meshing

According to the building size, the flow field calculation domain is selected as follows. The length L (x-direction), height H (z-direction) and width B (y-direction) are 2400m, 600m, and 1200m, respectively. The building model is arranged 800m away from the entrance in the x-direction, in the middle in the y-direction and on the lower side in the z-direction [18]. When the wind direction angle is 90°, the two towers are arranged in parallel, and the blocking rate in the calculation domain is 2.84%, which meets the requirements. Tetrahedral unstructured grid is adopted for grid division, and the grid near the building wall is encrypted. The minimum grid size is 2m, the computing domain is far away from the building area, and the maximum grid size is 25m. The grid size gradually transits from the building wall to the computing domain, with a total number of grids of about 1.6 million [19, 20].

2.3 Turbulence model

The research project is in S main urban area. This area belongs to an area with dense distribution of high-rise buildings. Meanwhile, the safety level of building structures in this area belongs to grade II [21]. Therefore, ω_n=0.4kN/m^2 is set. According to equation 1, the reference wind speed v_0 under the converted standard landform is:

$$v_0 = \sqrt{\frac{2\omega_0}{\rho}} = 25.3m/s \tag{1}$$

The dynamic viscosity of air is v=1.46×10-6m^2/s. The maximum height of the building is 220m, so the characteristic length is 220m, and the estimated Reynolds number is:

$$Re = \frac{v_0 L}{v} = 3.812 \times 10^8 \tag{2}$$

It is far beyond the critical Reynolds number of the flow around the plate, and the turbulence model should be used to simulate the flow field. After the comprehensive consideration, the turbulence model Shear Stress Transfer k $-\omega$ (SST k $-\omega$) is selected [22, 23].

The inlet of the numerical wind tunnel adopts a class D landform. The average wind speed profile, turbulence profile and turbulence parameters are programmed by user-defined functions (UDF) based on Fluent software as the interface of Fluent [24].

Wind speed profile of atmospheric boundary layer:

$$V(z) = V_{10}(\frac{350}{10})^{0.15}(\frac{z}{550})^{0.30} \tag{3}$$

Turbulence profile:

$$I(z) = 0.39(\frac{z}{10})^{-0.3} \tag{4}$$

Turbulence kinetic energy:

$$k = \frac{3}{2}(uI_z)^2 \tag{5}$$

Dissipation rating:

$$\varepsilon = C_\mu^{3/4}\frac{k^{3/2}}{l} \tag{6}$$

Specific dissipation rate:

$$\omega = \frac{k^{1/2}}{C_\mu^{1/4}l} \tag{7}$$

l represents the length of turbulence, and the value is 0.4. C_μ represents the turbulence scale, C_μ = 0.09. The wind speed profile of atmospheric boundary layer *V(z)*, specific dissipation rating ω, turbulence kinetic energy k and turbulent dissipation ε are realized by Fluent and UDF programming as the interface. The two sides and top of the basin are called symmetry boundary conditions similar to the free sliding wall. The outlet surface adopts pressure-outlet boundary conditions. The wall condition without sliding is adopted for the building surface and ground.

The first-order upwind scheme is used for the convection term in the initial calculation stage, and the second-order discrete scheme is adopted for the convection term in the later calculation stage to obtain more accurate numerical simulation results and rapid convergence [25, 26]. A fluent-3D separation implicit solver is used, and the COUPLED algorithm is used to solve iteratively. The criterion to judge the convergence of calculation is that the dimensionless residuals of all variables decrease and the variables reach stability. Meanwhile, the wind pressure of a certain point on the building surface is expressed as the average wind pressure coefficient. The wind pressure coefficient is defined as the ratio of the wind pressure at each measuring point to the undisturbed average wind pressure at the top of the model [27]. The expression is as follows:

$$\mu_i = \frac{P_i}{(1/2)\rho U_H^2} \tag{8}$$

μ_i represents the average wind pressure coefficient of measuring points on the building surface. P_i represents the average air pressure at the measuring point on the surface of the building. ρ represents the air density in the environment; U_H represents the average wind speed at the top of the turbulence model, as shown in equation 9:

$$U_H = V_{10}(\frac{350}{10})^{0.15}(\frac{z}{550})^{0.3} = 32.76m/s \tag{9}$$

2.4 Analysis of interference effect of wind load

The average wind pressure coefficient of a building surface is weighted average to study the overall stress of a building wall. The weighted average value is defined as the shape factor μ_s of the building wall. The expression reads:

$$\mu_s = \frac{\sum_i \mu_i A_i}{A} \tag{10}$$

A represents the total area of the surface of the building wall. A_i is the control area of a point on the surface of the building. μ_i is the average wind pressure coefficient at a certain point on the building surface.

In order to study the influence of the existence of adjacent buildings on the shape factor [28], the interference factor of the shape factor is defined as the ratio of the shape factor with interference to that without interference. According to the definition, there is the following expression:

$$IF_\mu = \frac{\mu_{sI}}{\mu_{sA}} \tag{11}$$

IF_μ represents the interference factor of the shape factor, μ_{sI} represents the shape factor with interference, and μ_{sA} represents the shape factor without interference [29].

The corresponding moment coefficient can be obtained by dimensionless treatment of the bending moment of the base. The expression reads:

$$C_{Mx} = \frac{M_x}{0.5\rho U_H^2 H^2 B} \tag{12}$$

$$C_{My} = \frac{M_y}{0.5\rho U_H^2 H^2 B} \tag{13}$$

$$C_{Mz} = \frac{M_z}{0.5\rho U_H^2 H^2 B} \tag{14}$$

B represents the width of the building, B=46m. ρ is the density of the air, ρ=1.225kg/m^3. H is the height of the building, H = 220m. C_{Mx}, C_{My}, and C_{Mz} represent the moment coefficient around x, y and z directions, respectively. M_x, M_y, and M_z represent the moment of the force around x, y and z directions, respectively. U_H is the undisturbed incoming wind speed at the top of the building, U_H=32.76 m/s.

In order to study the influence of adjacent buildings on the moment coefficient, the interference factor of the moment coefficient is defined as the ratio of the moment coefficient with interference to the moment coefficient without interference [30]. According to the definition, there is the following expression:

$$IF_M = \frac{C_{MI}}{C_{MA}} \tag{15}$$

IF_M represents the interference factor of the moment coefficient, C_{MI} represents the moment coefficient with interference, and C_{MA} represents the moment coefficient without interference [31].

3. Analysis of experimental results

3.1 Analysis of interference effect of average wind pressure coefficient

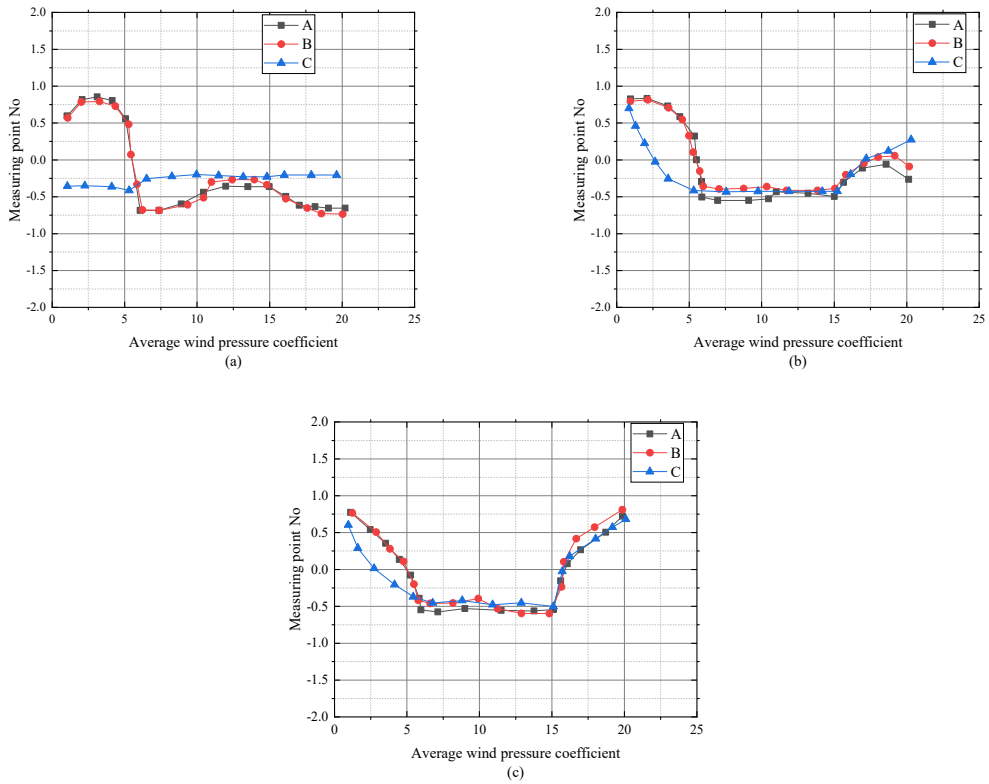

Figure 1. wind pressure distribution at section 2/3 (a: wind pressure distribution at 0° wind direction angle; b: wind pressure distribution at 45° wind direction angle; c: wind pressure distribution at 90° wind direction angle; A: single tower; B: tower D; C: tower E)

The following figures show the interference effect analysis of the average wind pressure coefficient according to the different sections of the two towers. Figure 1 and Figure 2 present the data results of wind pressure distribution comparison between the two towers at sections 2/3 and 1/3, respectively.

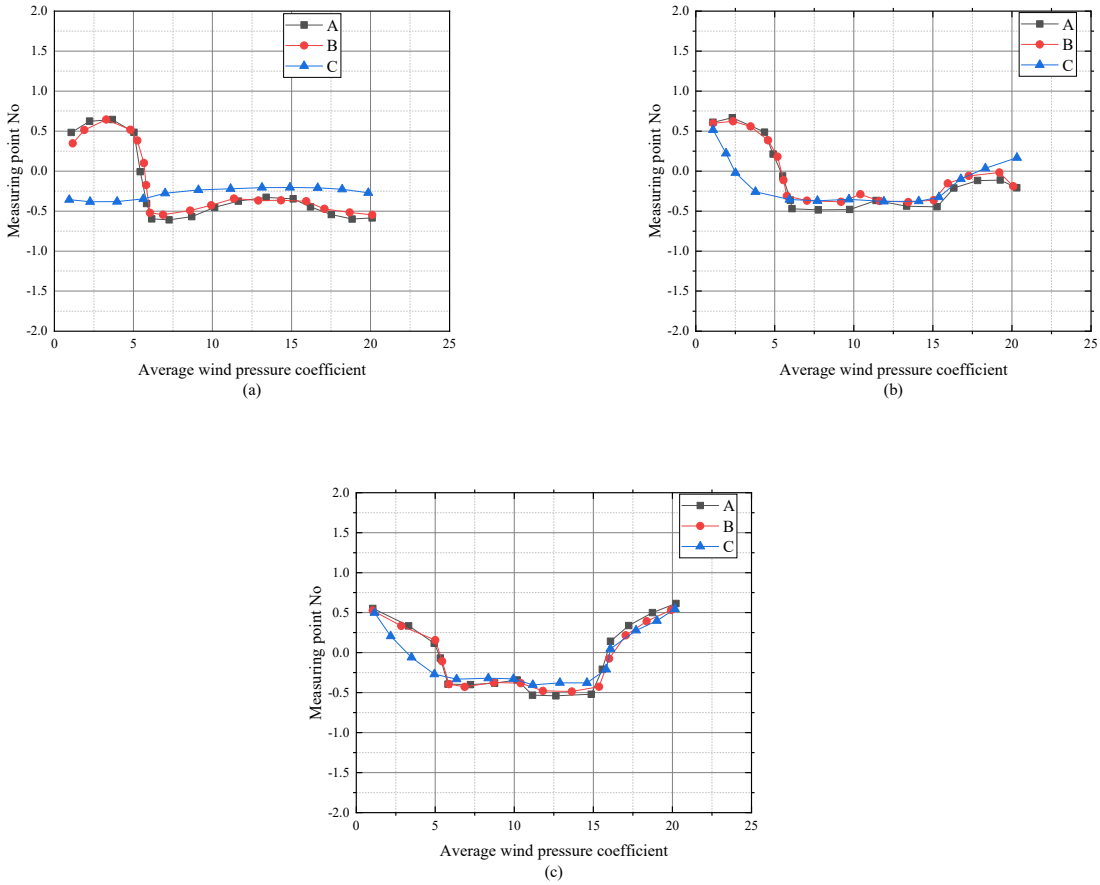

Figure 2. wind pressure distribution at 1/3 section (a: wind pressure distribution at 0° wind direction angle; b: wind pressure distribution at 45° wind direction angle; c: wind pressure distribution at 90° wind direction angle; A: single tower; B: tower F; C: tower G)

Figures 1 and 2 show that when the wind direction angle is 0° and there is shielding between two fabricated twin towers, the wind pressure on the windward surface of the upstream building will not be affected by the downstream building. However, due to the influence of upstream buildings, the surface wind pressure of downstream buildings is greatly reduced. When the wind direction angle changes to 90°, the two towers interfere with each other, resulting in a narrow channel effect. Such a narrow channel effect will increase the wind pressure on the walls of buildings on both sides of the narrow channel, which can be doubled at most.

3.2 Analysis of interference effect of building surface shape factor

Figure 3 shows the changes of interference factors and shape factors of prefabricated building surfaces under different wind direction angles.

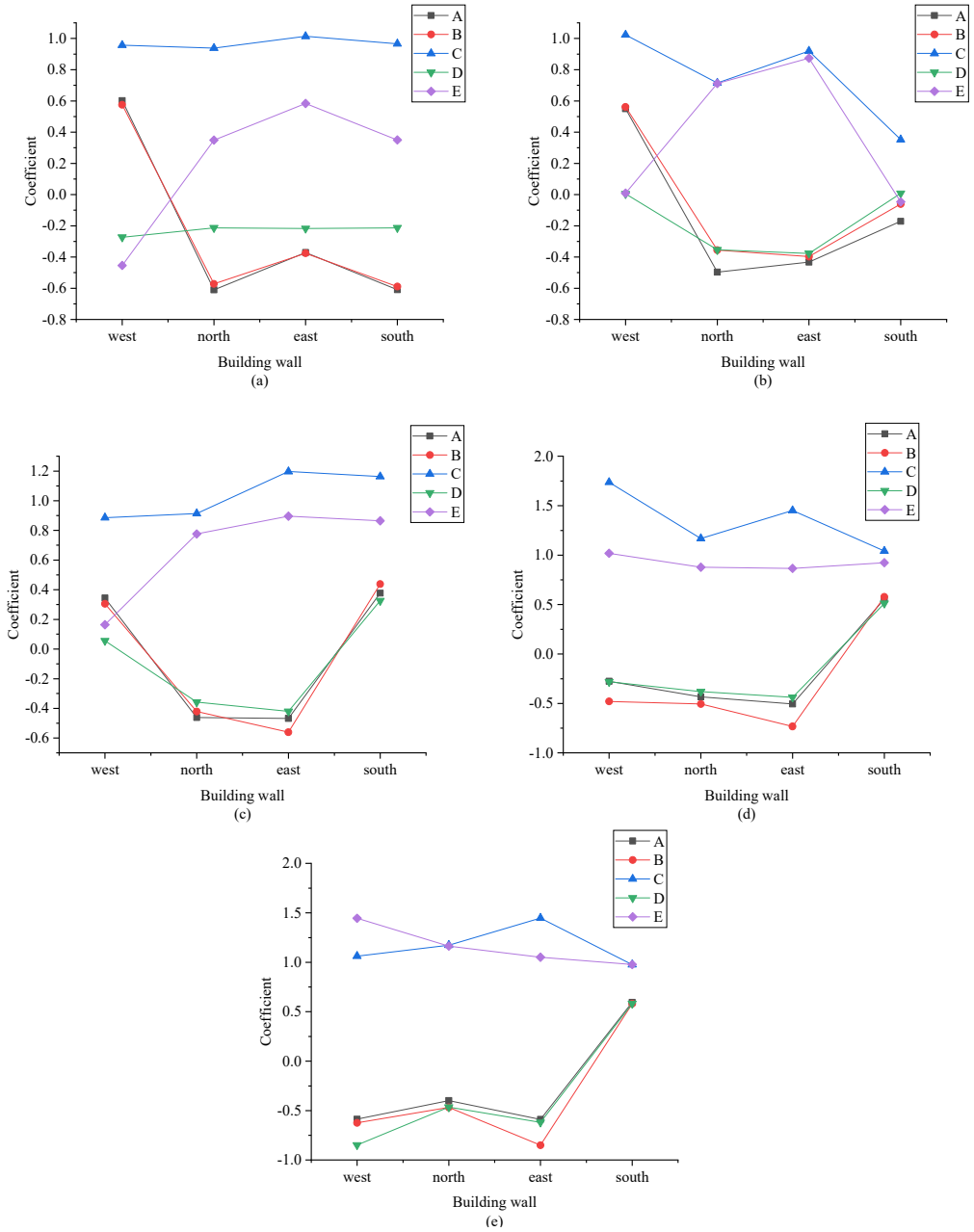

Figure 3. variation of interference factors and shape factors of prefabricated building surface under different wind direction angles (a: 0° wind direction angle; b: 22.5° wind direction angle; c: 45° wind direction angle; d: 67.5° wind direction angle; e: 90° wind direction angle; A: moment coefficient of the single tower; B: moment coefficient of tower F; C: moment coefficient interference factor of tower F; D: moment coefficient of tower G; E: moment coefficient interference factor of tower G)

3.3 Interference effect of base bending moment coefficient

Figure 4 shows the statistical results of the prefabricated building's base moment coefficient and interference factor under different wind direction angles.

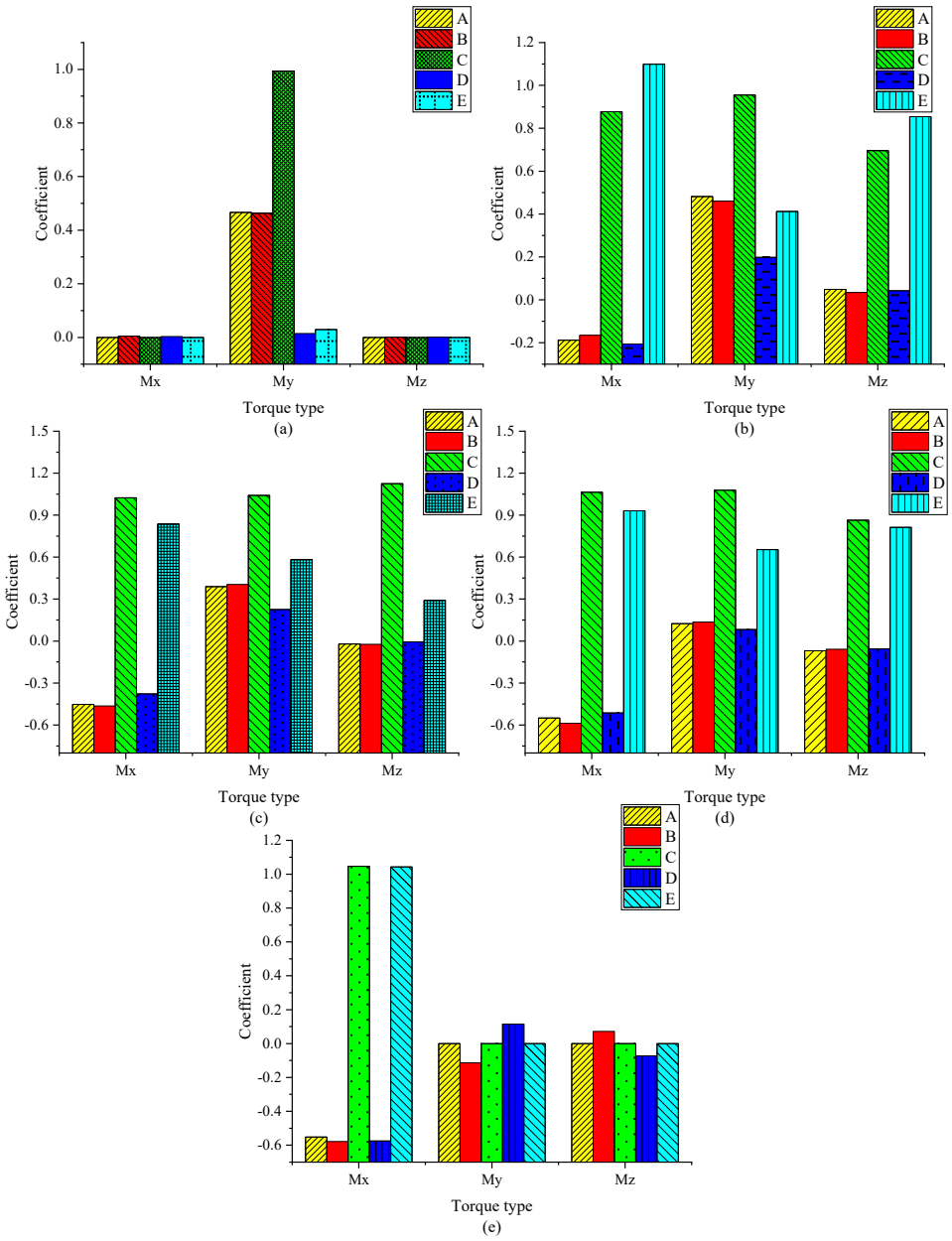

Figure 4. statistical results of base moment coefficient and interference factor of prefabricated buildings under different wind direction angles (a: 0° wind direction angle; b: 22.5° wind direction angle; c: 45° wind direction angle; d: 67.5° wind direction angle; e: 90° wind direction angle; A: moment coefficient of the single tower; B: moment coefficient of tower F; C: moment coefficient interference factor of tower F; D: moment coefficient of tower G; E: moment coefficient interference factor of tower G)

In the interference factor statistics of moment coefficient, tower F remains between 0.696 ~ 1.125 and tower G remains between 0.291 ~ 1.043. Therefore, the base bending moment of the two towers is analyzed from different wind direction angles. Under the condition of 0° wind direction angle, in the y-axis direction, the moment coefficient of a single tower is 0.466, and the maximum moment coefficient of tower G and tower F is 0.463. It is found that the moment coefficient of a single tower is slightly higher. In short, when the wind direction angle is 90° and 0°, it is most unsuitable for assembly work because when the wind direction angle is 90°, the building base torque and the base bending moment around the x-axis reach the maximum value simultaneously. If the moment around the y-axis is not 0, it will seriously affect the stress on the base of the building. When the wind direction angle is 0°, the mutual interference between the two towers has little effect on the base moment of the upstream building.

4. Conclusions

With the increasing number of high-rise prefabricated buildings in first-tier cities, the research on their safety has become more and more important. Therefore, numerical simulation analysis of the wind load of prefabricated buildings will be conducted based on the theory of fluid mechanics. First, the application results of wind load numerical simulation theory in different fields are analyzed. Then, the numerical model and turbulence model are established. The numerical simulation of building surfaces of a single tower, tower G and tower F is conducted under the same working conditions. Finally, the wind load interference effects of two fabricated towers and a single tower are analyzed. The experimental results show that when the wind direction angle is 0° and there is shielding between tower G and tower F, the wind pressure on the windward surface of the upstream building will not be affected by the downstream building. However, due to the influence of upstream buildings, the surface wind pressure of downstream buildings is significantly reduced. When the wind direction angle is 90°, tower G and tower F interfere with each other, resulting in the narrow channel effect. This narrow channel effect will increase the wind pressure on the walls of buildings on both sides of the narrow channel. Meanwhile, the wind pressure interference factor on the wall surface of prefabricated buildings remains between [-1, 1.5]. When the buildings in upstream are blocked, the wind pressure interference factor may become 0. However, the shape factor of negative pressure on the inner wall of the building will increase rapidly due to the narrow channel effect. The exploration here will provide a reference for relevant engineering teams to carry out prefabricated construction tasks and reduce the probability of accidents. However, the research scheme still has some limitations. If the fluctuating wind profile is used for numerical simulation analysis, more instantaneous data of buildings can be collected to make the experimental conclusion more accurate. Therefore, the calculation of fluctuating wind pressure can be considered in future research.

Acknowledgments

Funding Statement: This study was sponsored by the “Key Scientific and Technological Projects of Henan Higher Eduction” (Project name: Research and application of key welding technology for long-span steel box girder; grant number: 23B560015; https://hnapp.rcloud.edu.cn/articleAction/to_view.do?id=ff80808183356d5e018378f99fe6077e&sysMenu.menuId=C732244EA3550451E040007F010003CE; A. W).

Funding Statement: This study was sponsored by the “Key Scientific and Technological Projects of Henan Province 2022” (Project name: Research and application of key welding technology of fabricated u-ribbed stiffened steel bridge deck; grant number: 222102320267; http://kjt.henan.gov.cn/2022/01-27/2389939.html; A. W).

References

[1] Liang, Y., Yu, K., Pan, Z. (2021). Intergeneric and geomorphological variations in Symbiodiniaceae densities of reef-building corals in an isolated atoll, central South China Sea. Marine Pollution Bulletin, 163, 111946. doi: 10.1016/j.marpolbul.2020.111946.

[2] Moris, J. P., Kennedy, A. B., Westerink, J. J. (2021). Tsunami wave run-up load reduction inside a building array. Coastal Engineering, 3(1), 103910. doi: 10.1016/j.coastaleng.2021.103910.

[3] Suárez-Forero, D., Ardizzone, V., Silva, S. (2020). Quantum hydrodynamics of a single particle. Light: Science & Applications, 9(1), 13-14. doi: 10.1038/s41377-020-0324-x.

[4] Li, Y., Chen, L. (2020). The relationship between the internal condition and the ventilation environment in a modular building. Indoor and Built Environment, 30(3), 1420326X1989304. doi: 10.1177/1420326X19893044.

[5] Ritos, K., Kokkinakis, I. W., & Drikakis, D. (2018). Performance of high-order implicit large eddy simulations. Computers & Fluids, 173, 307-312. doi: 10.1016/j.compfluid.2018.01.030.

[6] Farmakis, P. S., Tsoutsanis, P., & Nogueira, X. (2020). WENO schemes on unstructured meshes using a relaxed a posteriori MOOD limiting approach. Computer Methods in Applied Mechanics and Engineering, 363, 112921. doi: 10.1016/j.cma.2020.112921.

[7] Niu, J. (2021). CFD Analysis of the Influence of Ionic Liquids on the Performances of a Refrigeration System. Fluid Dynamics and Materials Processing, 17(5),1003-1013. doi: 10.32604/fdmp.2021.015225.

[8] Gueydon, S., Bayati, I., Ridder, E. (2020). Discussion of solutions for basin model tests of FOWTs in combined waves and wind. Ocean Engineering, 209, 107288. doi: 10.1016/j.oceaneng.2020.107288.

[9] Seiler, L., Figueira, R., Schettini, C., Siegle, E. (2020). Three-dimensional hydrodynamic modeling of the Santos-So Vicente-Bertioga estuarine system, Brazil. Regional Studies in Marine Science, 37, 101348. doi: 10.1016/j.rsma.2020.101348.

[10] Vo, T. Q., Roelvink, D., Wegen, M., Reyns, J., Linh, V. (2020). Flooding in the Mekong Delta: the impact of dyke systems on downstream hydrodynamics. Hydrology and Earth System Sciences, 24(1), 189-212. doi: 10.5194/hess-24-189-2020.

[11] Yudin, R., Puzakov, R. (2021). Dynamic Model of the Drive Machines Forest Complex. Voronezh Scientific-Technical Bulletin, 4(4), 102-108. doi: 10.34220/2311-8873-2021-4-4-102-108.

[12] Sanz-Ronda, F. J. (2021). Turning Pools in Stepped Fishways: Biological Assessment via Fish Response and CFD Models. Water, 13, 1-4. doi: 10.3390/w13091186.

[13] Tt, A., Aw, A., Pl, B., SG, A., Dan, C., et al. (2020). Physical model investigation of mid-scale mangrove effects on flow hydrodynamics and pressures and loads in the built environment. Coastal Engineering, 162. 16-22. doi: 10.1016/j.coastaleng.2020.103791.

[14] Miao, S., Zhang, H., Tian, W. (2021). A Study on the Unsteady Flow Characteristics and Energy Conversion in the Volute of a Pump-as-Turbine Device. Fluid Dynamics and Materials Processing, 17(5), 1021-1036. doi: 10.32604/fdmp.2021.016925.

[15] Koch, R., Bastianello, A., Caux, J. S. (2021). Adiabatic formation of bound states in the one-dimensional Bose gas. Physical Review B, 103, 13-14. doi: 10.1103/PhysRevB.103.165121.

[16] Napreenko, K. S., Lamt, Y., Gina, A. V. (2021). Hydraulic losses optimization methods used in air conditioning system valve design for different closure angles. IOP Conference Series Materials Science and Engineering, 35(12), 012022. doi: 10.1088/1757-899X/1027/1/012022.

[17] Laouar, S., Delov, M. I., Litvintsova, Y., Kuzmenkov, D., Kutsenko, K. (2020). A thermohydraulic flow loop for developing novel solutions in the field of using digital twins for nuclear power facilities [in Russian]. Izvestiya Vysshikh Uchebnykh Zavedenii, 2, 122-134. doi: 10.26583/npe.2020.2.11.

[18] Wu, C., Nittrouer, J. A., Swanson, T., Ma, M., Allison, M. (2020). Dune-scale cross-strata across the fluvial-deltaic backwater regime: Preservation potential of an autogenic stratigraphic signature. Geology, 48(12), 3-5. doi: 10.1130/G47601.1.

[19] Dai, W., Bilal, A., Xie, Q. (2020). Numerical Modeling for Hydrodynamics and Near-Surface Flow Patterns of a Tidal Confluence. Journal of Coastal Research, 36(2), 295-312. doi: 10.2112/JCOASTRES-D-19-00058.1.

[20] Yuan, C., Wang, J., Pan, Y. (2021). Numerical Simulation of Wind Turbine Aerodynamic Characteristics under Wind Shear Based on Lattice-Boltzmann Method. E3S Web of Conferences, 248(4), 01070. doi: 10.1051/e3sconf/202124801070.

[21] Ong, R. H., Patruno, L., Yeo, D. (2020). Numerical simulation of wind-induced mean and peak pressures around a low-rise structure. Engineering Structures, 214, 110583. https://www.sciencedirect.com/science/article/pii/S0141029619336193.

[22] Micheli, L., Alipour, A., Laflamme, S. (2020). Multiple-Surrogate Models for Probabilistic Performance Assessment of Wind-Excited Tall Buildings under Uncertainties. ASCE-ASME Journal of Risk and Uncertainty in Engineering Systems Part a Civil Engineering, 6(4), 04020042. doi: 10.1061/AJRUA6.0001091.

[23] Jiang, Y., Bai, Y., Wang, C., Pang, X. (2021). Dynamic Response Analyses of Plastic Greenhouse Structure considering Fluctuating Wind Load. Advances in Civil Engineering, 21(3), 1-13. doi: 10.1155/2021/8886557.

[24] Rong, B., Yin, S., Wang, Q. (2021). Simulation and Analysis of Wind Pressure Coefficient of Landslide-Type Long-Span Roof Structure. Advances in Civil Engineering, 13, 1-15. doi: 10.1155/2021/8846568

[25] Sa, A., Mrg, A., Em, B. (2021). Numerical simulation of the Mexico wind turbine using the actuator disk model along with the 3D correction of aerodynamic coefficients in OpenFOAM - ScienceDirect. Renewable Energy, 163, 2029-2036. doi: 10.1016/j.renene.2020.10.120.

[26] Chao, Y., H,Yi. (2021) Experimental Analysis of a Pneumatic Drop-on-Demand (DOD) Injection Technology for 3D Printing Using a Gallium-Indium Alloy. Fluid Dynamics and Materials Processing, 17(3), 587-595. doi: 10.32604/fdmp.2021.015478.

[27] Li, X., Wang, J., Eftekhari, M. (2020). Improvement Strategies Study for Outdoor Wind Environment in a University in Beijing Based on CFD Simulation. Advances in Civil Engineering, 3(4), 1-14. doi: 10.1155/2020/8850254.

[28] Ishihara, T., Qian, G., Qi, Y. (2020). Numerical study of turbulent flow fields in urban areas using modified k-ε model and large eddy simulation. Journal of Wind Engineering and Industrial Aerodynamics, 206, 1-20. doi: 10.1016/j.jweia.2020.104333.

[29] Ding, J., Yin, W., Ma, Y. (2021). Large Eddy Simulation and Flow Field Analysis of Car on the Bridge under Turbulent Crosswind. Mathematical Problems in Engineering, 1(2), 1-10. doi: 10.1155/2021/7579696.

[30] Liang, X. F., Li, X. B., Chen, G. (2020). On the aerodynamic loads when a high speed train passes under an overhead bridge. Journal of Wind Engineering and Industrial Aerodynamics, 202, 104208. doi: 10.1016/j.jweia.2020.104208.

[31] Tsoutsanis, P., Kokkinakis, I. W., Könözsy, L., Drikakis, D., Williams, R. J., et al. (2015). Comparison of structured-and unstructured-grid, compressible and incompressible methods using the vortex pairing problem. Computer Methods in Applied Mechanics and Engineering, 293, 207-231. doi: 10.1016/j.cma.2015.04.010.